



Brain-wide Cas9-mediated cleavage of a gene causing familial Alzheimer's disease alleviates amyloid-related pathologies in mice

Yangyang Duan^{1,2,6}, Tao Ye^{1,2,3,4,6}, Zhe Qu⁵, Yuewen Chen^{1,3,4}, Abigail Miranda¹, Xiaopu Zhou^{1,2}, Ka-Chun Lok^{1,2}, Yu Chen^{1,2,3,4}, Amy K. Y. Fu^{1,2,3}, Viviana Gradinaru^{1,5} and Nancy Y. Ip^{1,2,3}✉

The pathology of familial Alzheimer's disease, which is caused by dominant mutations in the gene that encodes amyloid-beta precursor protein (APP) and in those that encode presenilin 1 and presenilin 2, is characterized by extracellular amyloid plaques and intracellular neurofibrillary tangles in multiple brain regions. Here we show that the brain-wide selective disruption of a mutated APP allele in transgenic mouse models carrying the human APP Swedish mutation alleviates amyloid-beta-associated pathologies for at least six months after a single intrahippocampal administration of an adeno-associated virus that encodes both Cas9 and a single-guide RNA that targets the mutation. We also show that the deposition of amyloid-beta, as well as microgliosis, neurite dystrophy and the impairment of cognitive performance, can all be ameliorated when the CRISPR-Cas9 construct is delivered intravenously via a modified adeno-associated virus that can cross the blood-brain barrier. Brain-wide disease-modifying genome editing could represent a viable strategy for the treatment of familial Alzheimer's disease and other monogenic diseases that affect multiple brain regions.

Alzheimer's disease (AD)—one of the most prevalent neurodegenerative diseases—is characterized by the deposition of amyloid-beta (A β) peptides and the presence of neurofibrillary tangles composed of hyperphosphorylated tau protein. Although the inherited forms of AD, termed familial AD, account for 3–5% of AD cases^{1–3}, their prevalence is comparable to that of other neurological diseases such as Huntington's disease⁴ and amyotrophic lateral sclerosis⁵. Familial AD is caused by fully penetrant and autosomal dominant mutations in the genes that encode APP as well as in those that encode catalytic components of the γ -secretase complex: presenilin 1 (PS1) and presenilin 2 (PS2)². Dysregulated processing of APP by γ -secretase causes the accumulation of A β peptides, which is a major factor in the disease pathogenesis⁶. Despite considerable advances in our understanding of the genetic causes of familial AD, there are currently no effective disease-modifying treatments.

Clustered regularly interspaced short palindromic repeats (CRISPR)–CRISPR-associated protein 9 (Cas9)-mediated genome editing is a powerful tool that is potentially capable of targeting specific mutations⁷. However, the development of CRISPR–Cas9 as a targeted genome-editing approach for disease-modifying familial AD therapies requires addressing the needs of widespread genome editing in the brain. Like most brain disorders, AD affects multiple brain regions including the cortex and the hippocampus^{8,9}. Current genome-editing strategies for brain disorders are delivered via intraparenchymal injection¹⁰, which affects limited brain regions with restricted beneficial outcomes. Therefore, an efficient and

global genome-editing method that can be used in the adult brain is urgently needed. Modified adeno-associated virus (AAV) variants that can cross the blood–brain barrier (BBB) have recently been developed, enabling widespread transduction in the central nervous system after intravenous delivery^{11–14}. Concordantly, brain-wide overexpression of a protein delivered via a BBB-crossing virus has been shown to promote recovery after ischaemic stroke in aged mice¹⁴. Therefore, modifying the expression of disease-modifier gene(s) in the central nervous system by administration of a BBB-crossing virus has potential for development as a therapeutic strategy for diseases such as familial AD. However, the ability of such a virus to deliver CRISPR–Cas9 genome-editing components to ameliorate the disease phenotypes has not yet been tested in vivo.

Given that most cases of familial AD are caused by monogenic mutations, CRISPR–Cas9-mediated genome editing has been used to disrupt or correct familial AD mutations and decrease A β production in vitro^{15,16}. Most patients with familial AD have a heterozygous disease-causing mutation², and humans that naturally carry one copy of APP, PSEN1 (which encodes PS1) or PSEN2 (which encodes PS2) do not exhibit obvious neurological symptoms^{17,18}. Thus, disruption of the disease-causing allele in patients with familial AD at the adult stage is a rational and feasible disease-modifying strategy for the treatment of familial AD. Among the familial APP mutations, the APP Swedish (APP^{SwE}) mutation (K670N/M671L) is located at the sequence that encodes the β -secretase cleavage site of APP; it makes the mutant APP more accessible for enzymatic cleavage, which results in higher A β production^{19–21}.

¹Division of Life Science, State Key Laboratory of Molecular Neuroscience, Molecular Neuroscience Center, Center for Stem Cell Research, The Hong Kong University of Science and Technology, Hong Kong, China. ²Hong Kong Center for Neurodegenerative Diseases, Hong Kong, China. ³Guangdong Provincial Key Laboratory of Brain Science, Disease and Drug Development, HKUST Shenzhen Research Institute, Shenzhen–Hong Kong Institute of Brain Science, Shenzhen, China. ⁴Chinese Academy of Sciences Key Laboratory of Brain Connectome and Manipulation, Shenzhen Key Laboratory of Translational Research for Brain Diseases, The Brain Cognition and Brain Disease Institute, Shenzhen Institute of Advanced Technology, Chinese Academy of Sciences, Shenzhen–Hong Kong Institute of Brain Science–Shenzhen Fundamental Research Institutions, Shenzhen, China. ⁵Division of Biology and Biological Engineering, California Institute of Technology, Pasadena, CA, USA. ⁶These authors contributed equally: Yangyang Duan, Tao Ye. ✉e-mail: boip@ust.hk

Although a recent study reports the feasibility of using genome editing to disrupt the *APP^{Swc}* mutation in transgenic mice carrying mutations on this gene, the low genome-editing efficiency of less than 3% prohibits the evaluation of the potential disease-modifying effect of disrupting this mutation¹⁶.

In this Article, we show that the AAV-mediated delivery of Cas9 and single-guide RNA (sgRNA) specifically targeting the *APP^{Swc}* mutation into the adult hippocampus generates efficient genome editing and alleviates multiple A β -associated pathologies in transgenic mouse models of A β deposition. Notably, this CRISPR-mediated beneficial effect persists for at least 6 months in the transgenic mice. Furthermore, a single systemic administration of a BBB-crossing AAV-Cas9 vector that targets the *APP^{Swc}* mutation ameliorates A β pathologies throughout the brain. Our results therefore demonstrate that systemic AAV administered in a single dose is a promising approach for the development of disease-modifying therapeutic interventions for familial AD. Moreover, such a strategy could be applicable to other disorders of the central nervous system that are caused by autosomal dominant mutations and affect multiple brain regions.

Results

CRISPR-Cas9-mediated genome editing specifically disrupts *APP^{Swc}* allele. We first targeted the *APP^{Swc}* double-base mutation (K670N/M671L) by designing two sgRNAs—SW1 and SW2—that place the mutation site within the first eight nucleotides immediately adjacent to the protospacer-adjacent motif (PAM) sequence (5'-NNGRRT-3') of Cas9 from *Staphylococcus aureus* (*SaCas9*) (Fig. 1a); this region is considered to be the 'seed sequence' region that is important for the recognition of Cas9-sgRNA²². Because mismatches between the sgRNAs and the wild-type (WT) sequence located in the seed sequence are poorly tolerated by Cas9²³, we expected SW1 and SW2 to distinguish the mutant *APP* sequence from the WT sequence. We validated the targeting specificities of the sgRNAs by using an EGxxFP reporter system²⁴ in HEK 293T cells (Fig. 1b). The expression of enhanced green fluorescent protein (EGFP) indicated that both SW1 and SW2 cleaved the *APP^{Swc}* sequence in the EGxxFP-*APP^{Swc}* reporter and not the *APP^{WT}* sequence in the EGxxFP-*APP^{WT}* reporter (Fig. 1c). This indicates that both SW1 and SW2 conferred high allele specificity to the *APP^{Swc}* mutation. Given that SW1 exhibits higher genome-editing efficiency in the EGxxFP-*APP^{Swc}* reporter and that SW1-mediated genome editing would disrupt the β -secretase cleavage site of APP (Fig. 1a), we chose SW1 for the subsequent genome-editing experiments. To confirm that the allele specificities of SW1 and SW2 were not due to their inability to edit the *APP^{WT}* allele, we generated two other sgRNAs—WT1 and WT2—to target the *APP^{WT}* allele at the same genetic loci as those corresponding to SW1 and SW2, respectively. The genome-editing efficiencies of WT1 and WT2 exceeded 50%, whereas neither SW1 nor SW2 induced any observable genome editing in HEK 293T cells carrying *APP^{WT}* alleles (Supplementary Fig. 1a,b), indicating that SW1 and SW2 specifically targeted the *APP^{Swc}* mutation. Moreover, examination of potential off-target effects among the top five computationally predicted off-target sites using the T7 endonuclease I mismatch assay detected no off-target activity in HEK 293T cells (Supplementary Fig. 1c,d).

To investigate the ability of the CRISPR-Cas9 system to disrupt the *APP^{Swc}* mutation in vivo, we packaged sgRNA SW1 together with Cas9 driven by the promoter elongation factor 1-alpha short (EFS) into a single AAV9 vector—denoted EFS::Cas9-SW1—and injected the virus into the hippocampi of 3-month-old 5XFAD mice (Fig. 1d). These 5XFAD mice harbour human *APP* cDNA with Swedish (encoding APP(K670N/M671L)), Florida (encoding APP(I716V)) and London (encoding APP(V717I)) mutations. The CRISPR-mediated genome editing of the *APP^{Swc}* mutation

can abolish the expression of full-length mutated APP and disrupt the effects of APP mutations. Four weeks post-injection, we collected the mouse brains for genomic analysis. AAV-mediated in vivo delivery of Cas9-SW1 efficiently edited the *APP^{Swc}* mutation in the virus-transduced brain regions (27% genome-editing efficiency; Fig. 1e,f and Supplementary Fig. 1e). This suggests that AAV-mediated administration of Cas9-SW1 efficiently disrupted the *APP^{Swc}* mutation in vivo.

We then examined the potential off-target events induced by Cas9-SW1 genome editing by performing whole-genome sequencing. A similar number of mutations (around 35,000) was detected in both the virus-transduced and the untransduced regions in individual mouse brains ($n=2$; Supplementary Fig. 1f and Supplementary Table 1), suggesting that off-target events induced by Cas9-SW1 editing are rare. We subsequently identified 257 somatic mutations residing in 46 genes as potential off-target events (Supplementary Fig. 1g and Supplementary Dataset). In particular, we identified 17 genes marked by 23 somatic mutations in exons or untranslated regions that might affect the regulation of gene expression and hence function (Supplementary Table 2). Of note, the cell-type-specific transcriptome analysis suggested that only three genes—*Sp110*, *Sp140* and *Abcg2*—were expressed in the mouse brain²⁵. Nonetheless, as these three genes were not prominently expressed in neurons²⁵, the identified mutations are unlikely to affect biological functions in the mouse brain.

Cas9-SW1 editing decreases amyloid-plaque burden in 5XFAD mice. To examine whether the disruption of the *APP^{Swc}* mutation in 5XFAD mice can decrease A β -associated pathologies, we delivered EFS::Cas9-SW1 via AAV injection into the hippocampus of 3-month-old 5XFAD mice, the age at which A β plaques start to accumulate without causing any apparent functional deficits²⁶. By 6 months of age, 5XFAD mice develop severe A β -associated pathologies characterized by elevated A β levels, A β plaque deposition, gliosis and neuronal dysfunction^{26–29} (Figs. 2–4). Three months after Cas9-SW1-mediated gene editing, the contents of both diethylamine-extracted soluble and formic acid-extracted insoluble A β in the dorsal hippocampal regions decreased (Fig. 2a) and the levels of both A β_{x-40} and A β_{x-42} species decreased by more than 60% (Fig. 2b,c).

We subsequently investigated whether the AAV-mediated expression of Cas9-SW1 affects amyloid-plaque deposition. Three months after the injection of Cas9-SW1, 6-month-old 5XFAD mice exhibited significantly lower A β plaque load in the virus-transduced hippocampal subregions when compared to the corresponding subregions of the uninjected side. Upon genome editing, the A β -positive areas decreased by 72.9% in the cornu ammonis (CA) region (Fig. 2d,f and Supplementary Fig. 2) and by 77.9% in the subiculum (Fig. 2e,g and Supplementary Fig. 2). The amyloid-plaque burden remained lower in 9-month-old 5XFAD mice (that is, 6 months post-injection); the A β -positive area decreased by 74.3% in the CA region (Fig. 2h,j and Supplementary Fig. 2) and by 83.6% in the subiculum (Fig. 2i,k and Supplementary Fig. 2). These results demonstrate that the effect of Cas9-SW1-mediated editing on amyloid pathology persisted for at least 6 months after a single administration (Fig. 2h–k and Supplementary Fig. 2).

Cas9-SW1 editing decreases gliosis in 5XFAD mice. In 5XFAD mice, A β pathology is accompanied by gliosis, which is characterized by increased numbers of activated microglia and astrocytes surrounding amyloid plaques²⁶. Therefore, we examined whether the lower amyloid-plaque burden observed in 5XFAD mice following genome editing is associated with decreased gliosis. In the subiculum of 5XFAD mice, which exhibits the most severe amyloid-plaque deposition (Supplementary Fig. 2), AAV-mediated

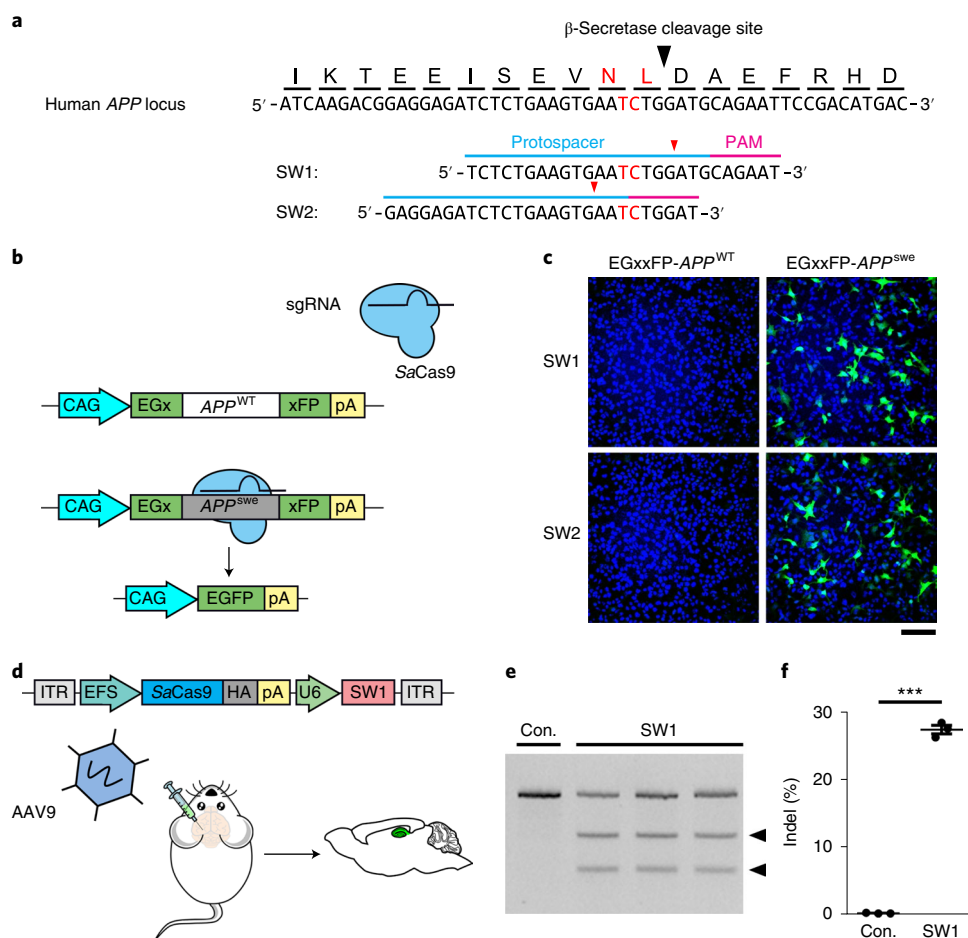


Fig. 1 | Design and validation of CRISPR-Cas9-mediated genome editing to disrupt the mutant APP^{swc} allele. **a**, The APP^{swc} double-base mutation (K670N/M671L) is close to the β -secretase site. Two sgRNAs—SW1 and SW2—were designed to target the APP^{swc} mutation using SaCas9. The arrowhead indicates the SaCas9 cleavage site. **b**, Schematic of the EGxxFP system used to analyse the editing efficiency of the CRISPR-Cas9 system in vitro. The APP^{WT} and APP^{swc} sequences were separately inserted between EGFP fragments with overlapping arms. SaCas9 (blue) editing resulted in homology-directed-repair-mediated DNA repair and reconstitution of the EGFP expression cassette, which yielded GFP signals. **c**, In vitro validation of allele-specific editing using the EGxxFP system. Cas9-SW1 and Cas9-SW2 were co-transfected with EGxxFP reporter plasmids containing APP^{WT} or APP^{swc} (EGxxFP- APP^{WT} or EGxxFP- APP^{swc}), respectively, into HEK 293T cells. Scale bar, 100 μ m. **d**, A single AAV vector, EFS::Cas9-SW1, was constructed to express haemagglutinin (HA)-tagged SaCas9 and sgRNA SW1 for intrahippocampal injection. ITR, inverted terminal repeat; pA, poly(A) tail; U6, human U6 promoter. **e**, T7 endonuclease I assay for AAV-mediated Cas9-SW1 editing in virus-transduced hippocampi from 5XFAD mice. Arrowheads indicate the CRISPR-Cas9-edited DNA fragments. Con., untransduced hippocampal region of 5XFAD mice. **f**, Percentage of insertion/deletion (indel) mutations. CRISPR-Cas9 editing led to the formation of such mutations, the percentage of which indicates the editing efficiency. Values are mean \pm s.e.m. $n = 3$ mice per group; *** $P < 0.001$; unpaired two-tailed t -test.

Cas9-SW1 editing led to decreases in microgliosis and astrogliosis. Specifically, in 5XFAD mice, disruption of the APP^{swc} allele decreased the proportion of microglia that were labelled by ionized calcium-binding adapter molecule 1 (Iba1) to 64.9% (Fig. 3a,b and Supplementary Fig. 3a). Although AAV-mediated Cas9-SW1 editing did not change the number of astrocytes that were positive for glial fibrillary acidic protein (GFAP) (Fig. 3c,d and Supplementary Fig. 3b), we observed a decrease in the GFAP-positive area (Fig. 3c,e and Supplementary Fig. 3b). These findings collectively suggest that, concurrent with the decreases in $A\beta$ levels and deposition, CRISPR-Cas9-mediated genome editing of familial AD mutations resulted in a decrease of gliosis, as indicated by fewer microglia and the decreased activation of astrocytes.

Cas9-SW1 editing improves neuronal functions in 5XFAD mice. To determine whether a single injection of AAV-mediated Cas9-SW1 can reverse the hippocampal synaptic-plasticity impairment

in 5XFAD mice, we measured the long-term potentiation (LTP). Compared to WT mice, LTP at Schaffer collateral-CA1 synapses was significantly impaired in 6-month-old 5XFAD mice; AAV-mediated Cas9-SW1 editing reversed the decrease of LTP by 90% (Fig. 4a,b). Furthermore, we demonstrated that AAV-mediated Cas9-SW1 editing increased the number of excitatory synapses in the subiculum of 5XFAD mice by 43.9%, as evidenced by co-staining for the presynaptic marker synaptophysin and the postsynaptic marker postsynaptic density 95 (PSD-95) (Fig. 4c-e). These results suggest that the genome editing reduced the loss of synapses in the transgenic mice.

Dystrophic neurites, which are swollen neuritic processes that surround amyloid plaques, also contribute to synaptic impairment in AD. Specifically, the aggregation of lysosomes in these neurites, which can be assessed by labelling with the lysosomal protein LAMP1, alters axonal transports and synaptic release properties, consequently disrupting synaptic communication³⁰⁻³².

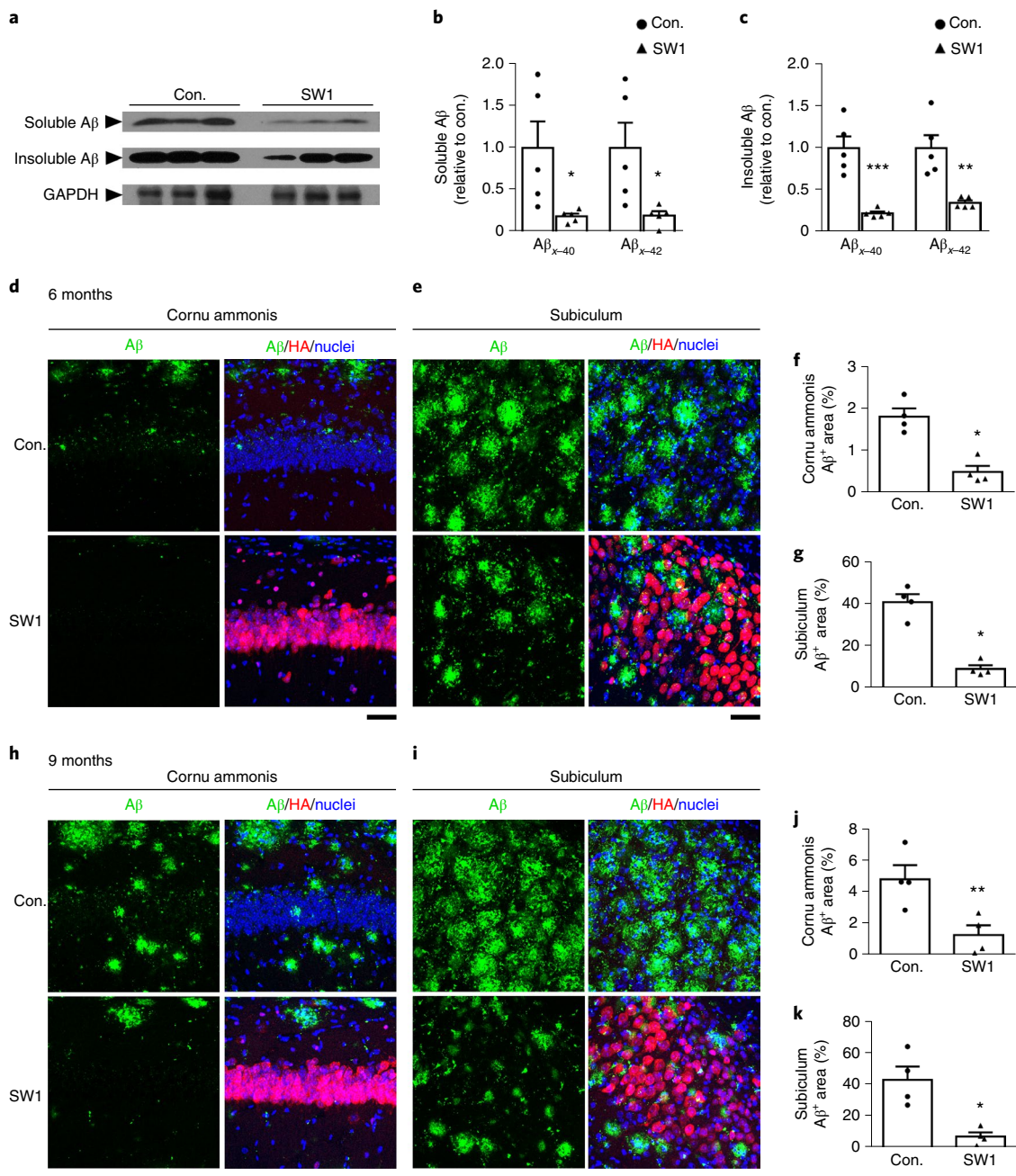


Fig. 2 | Intrahippocampal AAV-mediated Cas9-SW1 editing decreases the amyloid-plaque burden in 5XFAD mice. Intrahippocampal injection of AAV-mediated Cas9-SW1 in 3-month-old 5XFAD mice decreased A β levels and deposition. **a–c**, Soluble and insoluble A β contents in the dorsal hippocampal homogenates of 6-month-old 5XFAD mice after intrahippocampal injection of Cas9-SW1. **a**, Representative western blots of soluble and insoluble A β with GAPDH as a loading control. $n=3$ mice per group. **b,c**, Quantitative analysis of soluble and insoluble A β_{x-40} and A β_{x-42} by ELISA. Values are mean \pm s.e.m. $n=5$ mice per group; * $P=0.0342$ (soluble A β_{x-40}), * $P=0.0305$ (soluble A β_{x-42}), ** $P=0.0032$, *** $P<0.001$; unpaired two-tailed t -test. **d–k**, Amyloid-plaque deposition decreased in the hippocampal regions in 5XFAD mice that expressed AAV-mediated Cas9-SW1. Immunohistochemistry for A β (4G8; green), HA (red) and nuclei (blue). **d,e,h,i**, Representative images of distinct hippocampal regions (the cornu ammonis (**d,h**) and subiculum (**e,i**)) of 5XFAD mice at 6 months (**d,e**) and at 9 months (**h,i**) of age. Expression of the HA tag indicates Cas9 expression. Scale bars, 50 μ m. **f,g,j,k**, Quantification of A β -positive areas in the cornu ammonis (**f,j**) and subiculum (**g,k**). Values are mean \pm s.e.m. $n=4$ mice per group; * $P=0.0196$ (6 months; cornu ammonis), * $P=0.0102$ (6 months; subiculum), * $P=0.0103$ (9 months; subiculum), ** $P=0.0049$; paired two-tailed t -test.

Accordingly, AAV-mediated Cas9-SW1 editing in 5XFAD mice decreased the number of LAMP1-positive dystrophic neurites by approximately 50% (Fig. 4f,h and Supplementary Fig. 4) and increased the number of NeuN-positive neurons in the subiculum (Fig. 4g,i), suggesting that genome editing decreased neuronal loss.

Cas9-SW1 editing decreases A β pathologies in APP/PS1 mice. To examine the efficacy of the CRISPR-mediated disruption of the APP^{swc} mutation in transgenic mice with advanced disease status, we injected AAV-EFS::Cas9-SW1 into the hippocampus of APP/PS1 mice, a transgenic mouse model of A β pathology that has

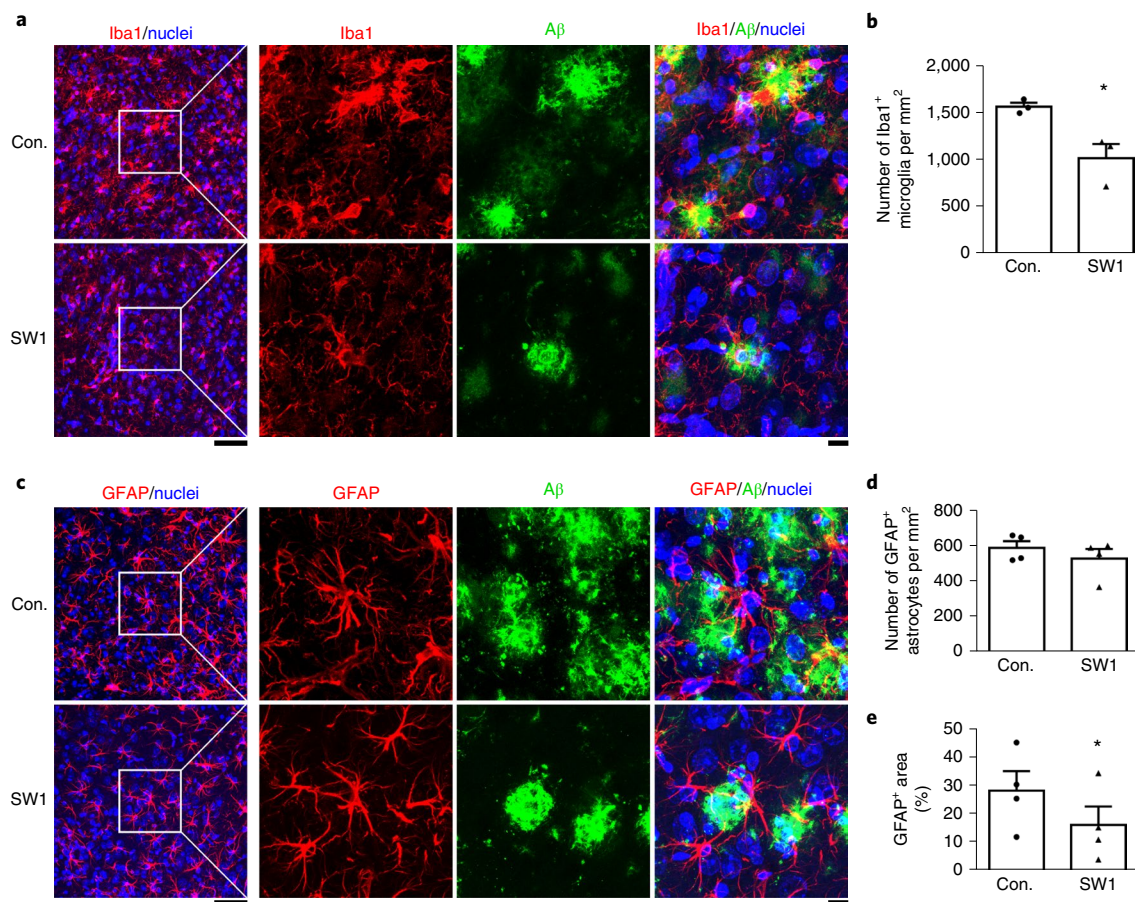


Fig. 3 | Intrahippocampal AAV-mediated Cas9-SW1 editing decreases gliosis in 5XFAD mice. a,b, AAV-mediated Cas9-SW1 editing decreased microgliosis in the hippocampus of 5XFAD mice. Immunohistochemistry for Iba1 (red), A β (4G8; green) and nuclei (blue) in 6-month-old 5XFAD mice. **a**, Representative images of the subiculum. Scale bars, 50 μ m (left); 10 μ m (right). **b**, Quantification of Iba1-positive cells. Values are mean \pm s.e.m. $n = 3$ mice per group; $*P = 0.0464$; paired two-tailed t -test. **c–e**, AAV-mediated Cas9-SW1 editing decreased the activation of astrocytes in the hippocampus in 5XFAD mice. Immunohistochemistry for GFAP (red), A β (4G8; green) and nuclei (blue) in 6-month-old 5XFAD mice. **c**, Representative images of the subiculum. Scale bars, 50 μ m (left); 10 μ m (right). **d,e**, AAV-mediated Cas9-SW1 editing in 5XFAD mice did not change the number of astrocytes but decreased astrocyte activation. **d**, Quantification of GFAP-positive cells. Values are mean \pm s.e.m. $n = 4$ mice per group; non-significant; paired two-tailed t -test. **e**, Percentage of area that is GFAP-positive. Values are mean \pm s.e.m. $n = 4$ mice per group; $*P = 0.0168$; paired two-tailed t -test.

a temporally different onset of disease phenotypes compared to 5XFAD mice. In the APP/PS1 mouse model, A β -plaque deposition and gliosis start to appear at approximately 4 months^{33,34}; LTP impairment and cognitive deficits are observed at 6 and 12 months, respectively^{35,36}. Accordingly, we injected AAV-EFS::Cas9-SW1 at 9 months of age (when the A β -associated pathologies and hippocampal synaptic dysfunctions are well developed) and collected the brains 6 months later. The genome-editing efficiency was 24% in APP/PS1 mice (Supplementary Fig. 5a,b), which is comparable to the value of 27% that was observed in 5XFAD mice. Moreover, after Cas9-SW1 administration, the amyloid-plaque burden was lower in the virus-transduced hippocampal regions of APP/PS1 mice than in the untransduced regions. Specifically, the amyloid-plaque burden in the CA and the subiculum of APP/PS1 mice decreased by 31.7% and 49.2%, respectively (Fig. 5a–d and Supplementary Fig. 5c,d). Concurrent with the decreased A β deposition, Cas9-SW1 editing approximately halved the number of Iba1-labelled microglia (Fig. 5e,f). We also observed fewer GFAP-labelled astrocytes (Fig. 5g,h) and a smaller GFAP-positive area (Fig. 5g,i). These results collectively suggest that CRISPR–Cas9-mediated genome editing decreased amyloid deposition and gliosis in transgenic mice with well-developed disease-associated phenotypes.

Systemic delivery of Cas9-SW1 globally decreases A β pathologies in 5XFAD mice. Given that hippocampal injection of AAV-EFS::Cas9-SW1 decreased A β -related pathologies in the virus-transduced regions (Figs. 2–4), we investigated the possibility of achieving Cas9-SW1-mediated genome editing throughout the brain. The recent development of a BBB-crossing AAV9 variant, AAV-PHP.eB¹¹, has made it possible to efficiently deliver Cas9-SW1 into the adult brain via systemic administration. Accordingly, we generated a BBB-crossing AAV-Cas9 vector driven by a neuron-specific human synapsin 1 (Syn) promoter, SW1-Syn::Cas9 (Supplementary Fig. 6a). Because systemic administration of this AAV vector resulted in only limited expression of Cas9 in the mouse brain (Supplementary Fig. 6b), we generated a virus construct that would result in enhanced expression of Cas9 in vivo. Specifically, inserting a truncated form of the woodchuck hepatitis virus post-transcriptional regulatory element (WPRE)³⁷ into the AAV construct (SW1-Syn::Cas9-mWPRE; Fig. 6a) markedly increased Cas9 expression in the hippocampus and cortex; it also kept the size of the construct within the approximately 5-kb package capacity of the AAV³⁸ (Supplementary Fig. 6a). With these optimizations, this BBB-crossing, neuron-specific, genome-editing system achieved a genome-editing efficiency in the brain that

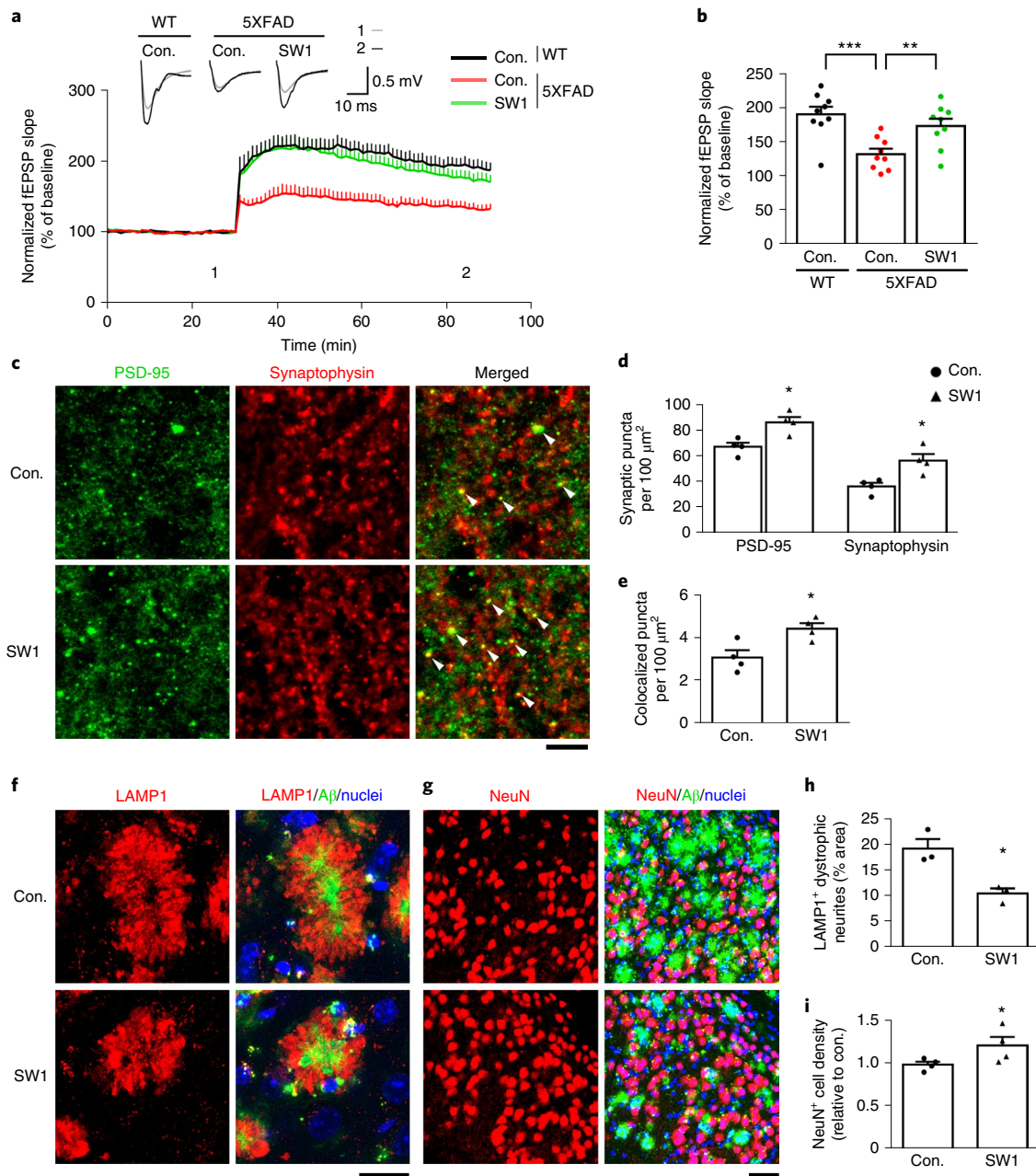


Fig. 4 | Intrahippocampal AAV-mediated Cas9-SW1 editing improves neuronal functions in 5XFAD mice. **a,b**, AAV-mediated Cas9-SW1 editing reversed the decrease of LTP in 6-month-old 5XFAD mice. LTP in the hippocampal CA1 region was induced by four trains of theta-burst stimulation. **a**, Averaged slopes of baseline-normalized field excitatory postsynaptic potential (fEPSP; mean \pm s.e.m.). Inset: examples of fEPSPs recorded 5 min before (1, grey) and 55 min after (2, black) LTP induction. **b**, Quantification of mean fEPSP slopes during the last 10 min of recording after LTP induction. Values are mean \pm s.e.m. WT Con., $n=9$ slices from 6 mice; 5XFAD Con., $n=9$ slices from 4 mice; 5XFAD SW1, $n=9$ slices from 5 mice; $**P=0.0063$, $***P<0.001$; unpaired two-tailed t -test. **c–e**, AAV-mediated Cas9-SW1 injection reduced the decrease of excitatory synapses (stained with PSD-95 (green) and synaptophysin (red)) in the subiculum of 9-month-old 5XFAD mice. **c**, Representative images. Scale bar, 5 μm . **d,e**, Quantification of PSD-95 puncta and synaptophysin puncta (**d**) and synaptophysin–PSD-95 co-localized puncta (**e**) in the subiculum. Values are mean \pm s.e.m. $n=4$ mice per group; $*P=0.0247$ (PSD-95), $*P=0.0125$ (synaptophysin), $*P=0.0390$ (co-localized puncta); paired two-tailed t -test. **f–i**, AAV-mediated Cas9-SW1 editing decreased neurite dystrophy and neuronal loss in the subiculum in 5XFAD mice. **f,g**, Co-staining with A β (4G8; green), nuclei (blue) and LAMP1 (a marker of neurite dystrophy; red) in 6-month-old 5XFAD mice (**f**) or NeuN (red) in 9-month-old 5XFAD mice (**g**). Scale bars, 50 μm (**f**); 200 μm (**g**). **h**, Quantification of LAMP1-positive dystrophic neurites. Values are mean \pm s.e.m. $n=3$ mice per group; $*P=0.0356$; paired two-tailed t -test. **i**, Quantification of NeuN-positive cell density. Values are mean \pm s.e.m. $n=4$ mice per group; $*P=0.0500$; paired two-tailed t -test.

was comparable to that achieved by intrahippocampal injection (Supplementary Fig. 7a,b).

Systemic delivery of Cas9-SW1 into 5XFAD mice using AAV-PHP.eB led to widespread expression of HA-tagged Cas9

throughout the brain (Supplementary Fig. 7c) and a decrease of amyloid-plaque deposition in various brain regions (Fig. 6b–d). In particular, the amyloid-plaque burden was not only decreased in the CA and the subiculum in the hippocampus (Fig. 6e–h and

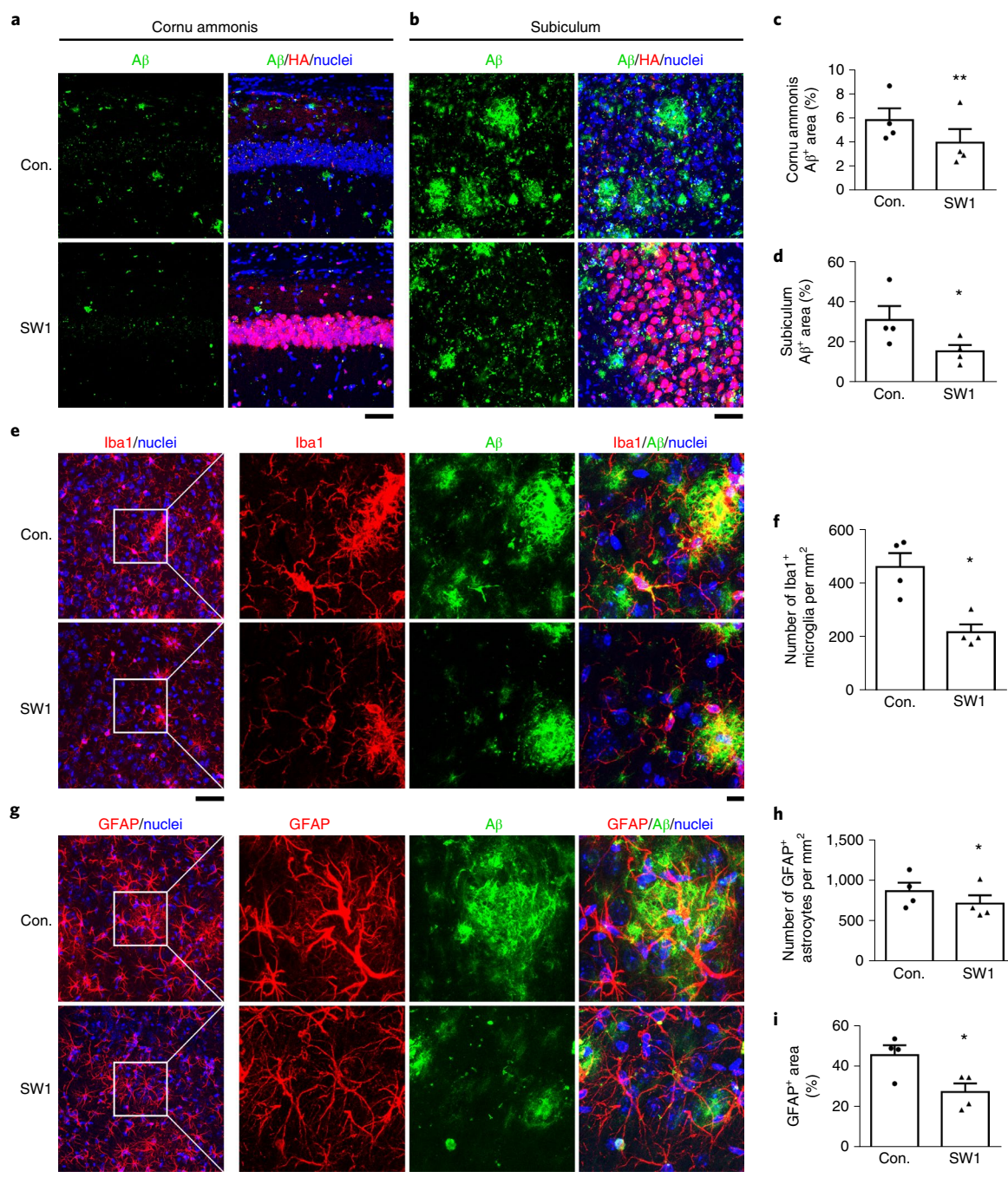


Fig. 5 | Intrahippocampal AAV-mediated delivery of Cas9-SW1 decreases pathologies associated with Alzheimer's disease in APP/PS1 mice.

Intrahippocampal injection of AAV-mediated Cas9-SW1 in 9-month-old APP/PS1 mice decreased Aβ deposition and gliosis. **a–d**, Amyloid-plaque deposition decreased in the hippocampal regions in APP/PS1 mice that expressed AAV-mediated Cas9-SW1. **a, b**, Immunohistochemistry for Aβ (4G8; green), HA (red) and nuclei (blue) in the cornu ammonis (**a**) and subiculum (**b**) of 15-month-old APP/PS1 mice. Scale bars, 50 μm. **c, d**, Quantification of Aβ-positive plaque areas in the cornu ammonis (**c**) and subiculum (**d**). Values are mean ± s.e.m. $n = 4$ mice per group; $*P = 0.0330$, $**P = 0.0025$; paired two-tailed t -test. **e–h**, AAV-mediated Cas9-SW1 editing decreased gliosis in the subiculum in APP/PS1 mice. **e**, Immunohistochemistry for microglial marker Iba1 (red), Aβ (4G8; green) and nuclei (blue). Scale bars, 50 μm (left); 10 μm (right). **f**, Quantification of Iba1-positive cells. Values are mean ± s.e.m. $n = 4$ mice per group; $*P = 0.0392$; paired two-tailed t -test. **g**, Immunohistochemistry for the astrocyte marker GFAP (red), Aβ (4G8; green) and nuclei (blue) in APP/PS1 mice. Scale bars, 50 μm (left); 10 μm (right). **h**, Quantification of GFAP-positive cells. Values are mean ± s.e.m. $n = 4$ mice per group; $*P = 0.0390$; paired two-tailed t -test. **i**, Percentages of GFAP-positive areas. Values are mean ± s.e.m. $n = 4$ mice per group; $*P = 0.0288$; paired two-tailed t -test.

Supplementary Fig. 7d), but also in the cortex (Fig. 6i, k) and in other brain regions, including the medulla of the brainstem (Fig. 6j, l and Supplementary Fig. 7c). Meanwhile, systemic injection of Cas9 with

a scrambled sgRNA (that is, AAV-PHP.eB:Con-Syn::Cas9-mWPRE) as a control did not cause any apparent adverse effects in either WT or 5XFAD mice. Specifically, the control virus induced neither

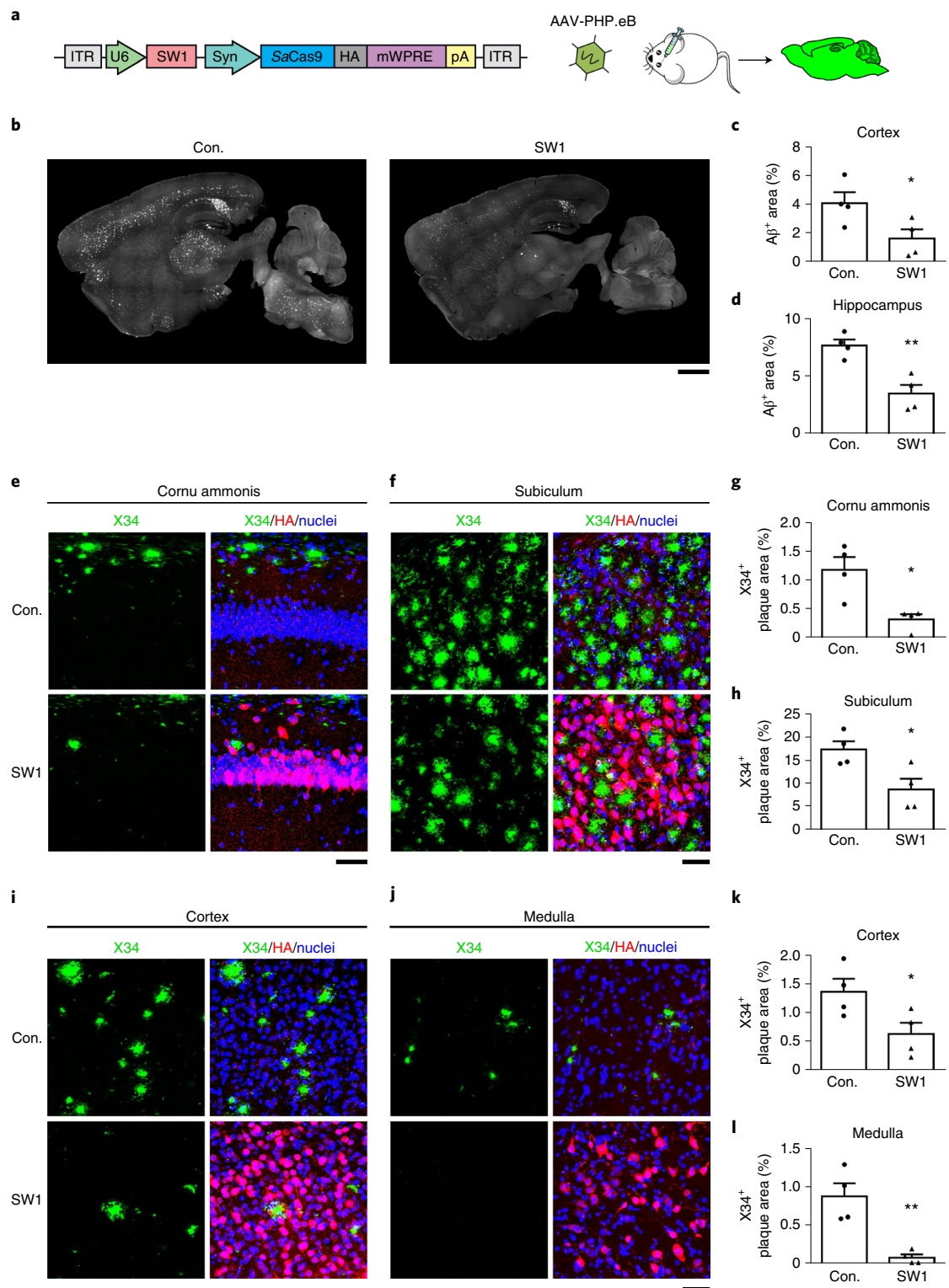


Fig. 6 | Systemic delivery of AAV-PHP.eB-mediated Cas9-SW1 globally decreases amyloid-plaque burden in 5XFAD mice. **a**, Diagram of brain-wide *APP*^{Swe} editing. A single AAV vector, designated SW1-Syn::Cas9-mWPRE, was designed to express HA-tagged SaCas9 and sgRNA SW1 for systemic administration using an AAV-PHP.eB capsid. **b–d**, Systemic injection of AAV-PHP.eB-mediated Cas9-SW1 into 3-month-old 5XFAD mice led to a global decrease in the A β -positive plaque area in the brain. **b**, Representative images of amyloid-plaque (4G8) staining in 6-month-old 5XFAD mice after injection of AAV-PHP.eB:SW1-Syn::Cas9-mWPRE. **c,d**, Quantification of amyloid-plaque areas in the cortex (**c**) and hippocampus (**d**). Values are mean \pm s.e.m. $n = 4$ mice per group; * $P = 0.0478$, ** $P = 0.0039$; unpaired two-tailed *t*-test. **e–l**, The decrease in X34-labelled amyloid-plaque burden was associated with Cas9 expression in the brain. **e,f,i,j**, Immunohistochemistry for X34 (green), HA (red) and nuclei (blue) in the cornu ammonis (**e**), subiculum (**f**), cortex (**i**) and medulla (**j**) in 6-month-old 5XFAD mice. Expression of the HA tag indicates Cas9 expression. Scale bar, 50 μ m. **g,h,k,l**, Quantification of X34-labelled plaque areas in the in the cornu ammonis (**g**), subiculum (**h**), cortex (**k**) and medulla (**l**). Values are mean \pm s.e.m. $n = 4$ mice per group; * $P = 0.0120$ (cornu ammonis), * $P = 0.0254$ (subiculum), * $P = 0.0471$ (cortex), ** $P = 0.0039$; unpaired two-tailed *t*-test.

gliosis nor behavioural deficits in WT mice (Supplementary Fig. 8a–f). Moreover, the control virus did not affect the amyloid-plaque burden in 5XFAD mice (Supplementary Fig. 8g–i). Thus, our results collectively demonstrate that systemic administration of Cas9-SW1 decreased A β pathologies in multiple brain regions of 5XFAD mice.

Systemic delivery of Cas9-SW1 decreases A β -associated pathologies and improves cognitive performance in 5XFAD mice. After systemic Cas9-SW1 editing, 5XFAD mice exhibited fewer Iba1-labelled microglia (Fig. 7a,b) and LAMP1-positive dystrophic neurites in the subiculum (Fig. 7d,e). This suggests that the systemic delivery of Cas9-SW1 globally decreased A β -associated phenotypes, including microgliosis and neurite dystrophy, in 5XFAD mice.

Previous studies report that transgenic mouse models of A β deposition exhibit impaired habituation and working memory as well as increased risk-taking behaviour^{26,35,39,40}. Given that the systemic delivery of Cas9-SW1 globally decreased amyloid-associated pathologies, we assessed its beneficial effects on the habituation ability, working memory and risk-taking behaviour of 5XFAD mice by using the exploratory open-field test, the Y-maze spontaneous-alternation test and the elevated plus maze test, respectively.

In the open-field test, the 5XFAD mice exhibited significantly slower habituation to the novel testing environment than the WT mice during the 3-day training period. In contrast to the uninjected 5XFAD mice, the mice that received Cas9-SW1 exhibited significantly improved habituation to the testing environment (Fig. 7e).

The Y-maze test measures the working memory of mice by allowing them to explore three arms of the maze. The ability of mice to alternate the arms into which they enter requires intact working memory (to remember which arm they previously visited). Compared to the WT mice, 5XFAD mice exhibited a significantly smaller percentage of spontaneous alternation among all entries (Fig. 7f). Meanwhile, 5XFAD mice that received Cas9-SW1 exhibited a significantly greater percentage of spontaneous alternation than those that did not receive Cas9-SW1 (Fig. 7f).

The elevated plus maze test examines the risk-taking behaviour and the explorative drive of mice by evaluating their exploration of open anxiogenic areas^{39,40}. The 5XFAD mice spent more time in the open arms than did the WT mice, whereas the 5XFAD mice that received Cas9-SW1 spent significantly less time in the open arms compared to the uninjected 5XFAD mice (Fig. 7g). These results collectively suggest that systemic delivery of Cas9-SW1 improved the cognitive performance of the 5XFAD mice.

Discussion

In this study, we show that a single injection of AAV-Cas9 vector selectively and efficiently edited the human *APP^{swc}* allele in vivo, alleviating A β -associated pathologies in transgenic mouse models of A β deposition. By using an improved BBB-crossing AAV vector, AAV-PHP.eB¹¹, systemic administration of this CRISPR-Cas9 system in transgenic mice achieves efficient genome editing in multiple brain regions and exerts a global beneficial effect, ameliorating A β deposition, microgliosis and neurite dystrophy as well as improving cognitive functions. Overall, systemic AAV delivery targeting a disease-causing mutation at the adult stage resulted in efficient brain-wide genome editing, consequently alleviating disease phenotypes throughout the brain.

Among the familial AD mutations, *APP^{swc}* is a double-point mutation located in the seed sequence of *SaCas9*. This enables selective target recognition and also makes it an ideal candidate for allele-specific editing, because the mismatches between the sgRNA and genomic DNA in the seed sequence region are poorly tolerated by Cas9 nuclease²². Although selective disruption of the mutated allele of *APP^{swc}* has been achieved in the hippocampus in a transgenic mouse model of A β deposition by using two AAVs that express an

APP^{swc}-specific sgRNA and Cas9 nuclease from *Streptococcus pyogenes* (*SpCas9*; 1,368 amino acids), respectively, the genome-editing rate of that CRISPR-Cas9 system on the familial AD mutant allele was less than 3%¹⁶. Therefore, to increase the editing efficiency of Cas9, we used a CRISPR-Cas9 system that can be packaged into an all-in-one AAV vector with the smaller *SaCas9* (1,053 amino acids) and its sgRNA, instead of the two vectors used for *SpCas9*⁴¹. Accordingly, we improved the in vivo editing efficiency of the CRISPR-Cas9 system to around 30%. Although the *APP^{swc}* mutation accounts for only a small proportion of familial AD cases, other familial AD mutations—such as that encoding the mutant protein PS1(L166P)—are also amenable to allele-specific gene disruption. More than 200 dominant disease-causing mutations in *APP*, *PSEN1* and *PSEN2* have been identified to date⁴². Moreover, the development of the *SaCas9* variant—which possesses alternative PAM compatibility⁴³—has expanded the targeting range of the CRISPR-Cas9 system, thereby broadening the range of nucleotide sequences in familial AD mutations that could be candidates for allele-specific disruption. Although familial AD accounts for only approximately 3–5% of the total cases of AD^{1–3}, this CRISPR-Cas9-mediated gene approach still has immense potential for therapeutic development for the treatment of familial AD.

Although two recent studies have demonstrated that CRISPR-Cas9-based strategies can ameliorate A β -associated phenotypes in transgenic mouse models, their translation to the clinic may incur challenges. In one study, decreasing APP expression in the germline of *APP*-knock-in mice using a CRISPR-Cas9 system alleviated the amyloid-plaque burden⁴⁴. However, it might not be possible to translate germline editing to an intervention strategy for AD. The other study used CRISPR-Cas9-mediated genome editing to knock out β -secretase 1 in the hippocampus of adult transgenic mice to alleviate A β -associated pathologies⁴⁵. However, β -secretase 1 is not a good target for clinical applications, because its inhibition can cause detrimental effects such as the impairment of synaptic function and cognitive behaviours^{46–48}. In this study, we show that CRISPR-Cas9-mediated disruption of the *APP^{swc}* allele ameliorates not only amyloid-plaque deposition but also gliosis, synaptic dysfunctions and cognitive impairment in transgenic mouse models of A β deposition. Disruption of the disease-causing allele in familial AD patients in the adult stage is therefore a promising disease-modifying strategy for the treatment of familial AD.

Our study also effectively addresses one major challenge of developing CRISPR-Cas9 systems for AD therapy: the need for brain-wide genome editing. AD affects multiple brain regions, but current delivery methods into the adult brain (both viral and nonviral) require intraparenchymal injection¹⁰, which limits the region that can be edited by Cas9. Single-site hippocampal injection of AAV9 infects only part of the hippocampus. Thus, the insufficient delivery of the CRISPR-Cas9 system may negate its potential beneficial effects. Efficient brain-wide delivery of genome-editing components is therefore urgently needed for therapeutic development of the CRISPR-Cas9 system for familial AD. We modified the AAV-PHP.eB BBB-crossing virus¹¹ with the CRISPR-Cas9 system to edit the *APP* gene in vivo. Importantly, we used a neuron-specific promoter to drive the expression of Cas9 to achieve neuron-specific genome editing, because A β is mainly produced by APP-expressing neurons. This system disrupts only the mutated *APP* in neurons, which mitigates the potential safety issue caused by Cas9 editing, because post-mitotic neurons cannot divide. With the optimization of the Cas9 expression construct (that is, the insertion of a truncated WPRE element into the AAV vector construct to enhance Cas9 expression), our PHP.eB-mediated CRISPR-Cas9 system achieved a global editing rate in the brain that was comparable to that achieved by local intrahippocampal injection. Although AAV-PHP.eB is limited to certain strains of mice, engineered vectors are emerging that can transduce previously resistant strains—such as BALB/c—and

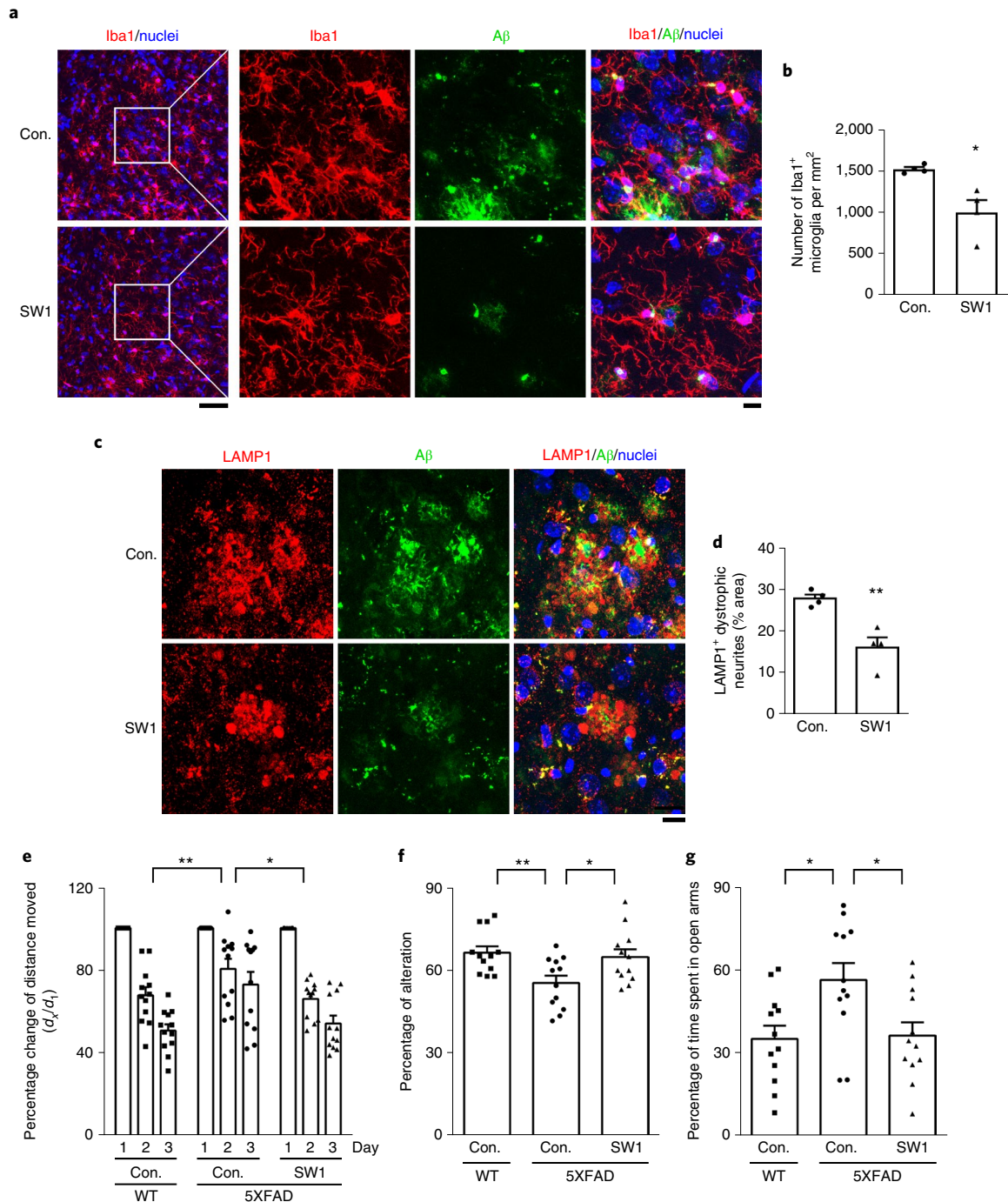


Fig. 7 | Systemic delivery of AAV-PHP.eB-mediated Cas9-SW1 decreases microgliosis and neurite dystrophy, and improves cognitive performance in 5XFAD mice. **a,b**, Systemic delivery of AAV-PHP.eB-mediated Cas9-SW1 in 3-month-old 5XFAD mice decreased microgliosis in the subiculum. **a**, Immunohistochemistry for Iba1 (red), A β (4G8; green) and nuclei (blue) in 6-month-old 5XFAD mice. Scale bars, 50 μ m (left); 10 μ m (right). **b**, Quantification of Iba1-positive microglia. Values are mean \pm s.e.m. $n = 4$ mice per group; $*P = 0.0130$; unpaired two-tailed t -test. **c,d**, AAV-PHP.eB-mediated Cas9-SW1 editing decreased neurite dystrophy in 5XFAD mice. **c**, Representative images showing staining for LAMP1 (a marker of neurite dystrophy; red), A β (4G8; green) and nuclei (blue) in the subiculum in 6-month-old 5XFAD mice. Scale bar, 10 μ m. **d**, Quantification of LAMP1-positive dystrophic neurites. Values are mean \pm s.e.m. $n = 4$ mice per group; $**P = 0.0040$; unpaired two-tailed t -test. **e-g**, Systemic delivery of AAV-PHP.eB-mediated Cas9-SW1 improved the cognitive performance of 5XFAD mice. **e**, Systemic delivery of AAV-PHP.eB-mediated Cas9-SW1 improved habituation in the exploratory open-field test. The graph shows the percentage change in the distance travelled (d_x) relative to that travelled on the first day of training (d_1). Values are mean \pm s.e.m. $n = 12$ mice per group; $*P = 0.0265$, $**P = 0.0099$; two-way repeated-measures ANOVA. **f**, Systemic delivery of AAV-PHP.eB-mediated Cas9-SW1 improved spatial working memory in the spontaneous-alteration Y-maze test. Values are mean \pm s.e.m. $n = 12$ mice per group; $*P = 0.0242$, $**P = 0.0049$; unpaired two-tailed t -test. **g**, Upon systemic delivery of AAV-PHP.eB-mediated Cas9-SW1, the 5XFAD mice spent significantly less time in the open arms in the elevated maze test. Values are mean \pm s.e.m. $n = 12$ mice per group; $*P = 0.0123$ (WT control versus 5XFAD control), $*P = 0.0173$ (5XFAD control versus 5XFAD SW1); unpaired two-tailed t -test.

other species such as marmosets^{49,50}. Given these ongoing developments, our work is a proof-of-concept towards genome-editing therapy using systemic delivery vectors.

To bolster the therapeutic development of CRISPR-mediated genome editing, it is important to evaluate the potential off-target events induced by genome editing. Herein, comparison of the whole-genome sequencing data of virus-transduced and untransduced brain regions within an individual mouse suggested that off-target events induced by Cas9-SW1 editing are rare, as the number of the mutations in virus-transduced regions was close to the basal number in the untransduced regions. After prioritizing the mutations according to their genomic locations and the brain expression of corresponding genes, we narrowed the potential off-target events of Cas9-SW1 to three genes expressed in the brain—*Sp110*, *Sp140* and *Abcg2*—for which expression levels might be affected. *Sp110* and *Sp140* belong to the nuclear body protein family and potentially regulates gene transcription⁵¹, whereas *Abcg2* belongs to the ATP-binding cassette transporter superfamily and serves as a xenobiotic exporter⁵². Notably, these genes are not prominently expressed in neurons²⁵. As the synapsin-driven Cas9 system can target only the neurons, these mutations are unlikely to affect the expression and hence the functions of these genes in neurons. Therefore, the biological effects of these potential off-target mutations are likely to be minimal. Furthermore, our findings also underscore the importance of an unbiased and comprehensive analysis of potential off-target events, such as whole-genome sequencing, for the development of CRISPR–Cas9-mediated gene therapy.

In summary, we applied a BBB-crossing, AAV-mediated, CRISPR–Cas9-based strategy to selectively and efficiently edit a disease-causing allele *in vivo*. Our proof-of-concept study shows that the brain-wide editing of the mutated *APP^{swc}* allele led to persistent beneficial effects *in vivo*, including alleviation of A β -associated pathologies, which makes it a promising strategy for further development. We believe that the AAV-mediated, single-dose, non-invasive CRISPR–Cas9 system represents a promising approach to address the lack of therapeutic options for familial AD, as well as for other forms of brain disease that are caused by dominant mutations that affect multiple brain regions.

Methods

Molecular cloning and GFP reporter assay. We adapted the AAV packaging construct from pX601-AAV-CMV::NLS-SaCas9-NLS-3xHA-bGHpA;U6::BsaI-sgRNA (Zhang Lab; Addgene plasmid 61591)⁴¹. For intrahippocampal injection, we replaced the cytomegalovirus (CMV) promoter with the EFS promoter. For systemic injection, we used a modified pX601 construct in which the promoter was replaced with the human Syn gene promoter and a truncated form of the WPRE cassette (Addgene plasmid 61463) was added to enhance Cas9 expression³⁷. Moreover, we replaced bovine growth hormone poly(A) (bGHpA) with synthetic poly(A). We inserted the sgRNAs into the construct by BsaI sites. The sequences of the sgRNAs are listed in Supplementary Table 3.

To evaluate the genome-editing efficiency of Cas9-sgRNA, we used the GFP reporter construct pCAG-EGxFP (Addgene plasmid 50716)³⁴, provided by M. Ikawa. We inserted the *APP^{swc}* and *APP^{wt}* alleles by ligating oligos into BamHI and EcoRI sites. We mixed 1 μ g Cas9-sgRNA with 1 μ g pCAG-EGxFP-APP and transfected the mixture into HEK 293T cells using Lipofectamine 3000 (Thermo Fisher Scientific). We examined the resultant GFP expression by fluorescence microscopy 12 h post-transfection.

Mice. We obtained 5XFAD transgenic mice, which harbour five familial AD mutations (*APP*(K670N/M671L)), Florida (encoding *APP*(I716V)) and London (encoding *APP*(V717I)) mutations, and mutations encoding PS1(M146L/L286V)²⁶; and *APP*/PS1 transgenic mice, which harbour the *APP* Swedish mutation (encoding *APP*(K670N/M671L)) and *PSEN1* exon 9 deletion³³, from the Jackson Laboratory (stock no. 008730 and 004462, respectively). All experiments were conducted using male 5XFAD mice or female *APP*/PS1 mice. All mice were housed in the Animal and Plant Care Facility at the Hong Kong University of Science and Technology. The Animal Ethics Committee of the Hong Kong University of Science and Technology approved all animal experiments.

Intrahippocampal and systemic injection of AAV. For AAV used in intrahippocampal injections, AAV9-Cas9-SW1 was generated by the Vector

Core at the University of North Carolina at Chapel Hill and titred by dot blot. We anaesthetized 3-month-old mice with isoflurane and injected 6×10^{10} vector genomes (vg) virus per mouse (2 μ l of 3×10^{13} vg ml⁻¹). We used the following coordinates (relative to the bregma) to target the CA1 region of the hippocampus: anteroposterior (AP), -2.0 mm; mediolateral (ML), -1.7 mm; dorsoventral (DV), -1.4 mm (ref. ⁵³). Given that intrahippocampal injection of empty AAV9 vector does not generate adverse effects in mice^{54–56}, the uninjected side of the same mouse served as the control. We euthanized the mice 3 or 6 months after virus injection.

For AAV used in systemic delivery, we generated AAV-PHPeB:Cas9-Con and AAV-PHPeB:Cas9-SW1 as previously described³⁷ and titred them by quantitative polymerase chain reaction (qPCR). We anaesthetized 3-month-old mice and injected the virus retro-orbitally at a dose of 1×10^{13} vg per mouse (100 μ l of 1×10^{14} vg ml⁻¹). We euthanized the mice at 6 or 9 months of age to analyse A β -associated pathologies.

T7 endonuclease I assay. We performed the T7 endonuclease I mismatch assay to analyse editing efficiency. In brief, we dissected the subiculum and cornu ammonis regions from 300- μ m-thick hippocampal slices and extracted the genomic DNA using QuickExtract DNA Extraction Solution (Epicentre Biotechnologies, QE09050). Amplified DNA was denatured and reannealed from 95 °C to room temperature. We subsequently added T7 endonuclease I (New England Biolabs, M0302) and incubated the mixture at 37 °C for 15 min. We analysed the products using 2.5% agarose gel electrophoresis for visualization. Next, we quantified the intensity of enzyme-cut and enzyme-uncut bands using ImageJ (NIH) software. Finally, we calculated the editing efficiency as follows:

$$\text{Editing efficiency (\%)} = 1 - \sqrt{1 - \frac{\text{cut bands}}{(\text{uncut band} + \text{cut bands})}} \times 100$$

Genome sequencing and bioinformatics analysis. We extracted genomic DNA using the E.Z.N.A. Tissue DNA Kit (Omega Bio-tek) and subjected it to the Illumina NovaSeq system (Novogene) for whole-genome sequencing (50 \times). We subjected raw reads (150 bp paired-end) to the Trimmomatic (v.0.32) for the trimming and filtering of low-quality reads. The reads that passed quality control were mapped to a modified version of the mouse reference genome (UCSC mm10) with the further inclusion of sequences for human *APP* and *PSEN1* using BWA mem (v.0.7.12-r1039). Germline and somatic mutations were genotyped following the Genome Analysis Toolkit (GATK) Best Practices (v.4.1.2.0) using the default setting. Specifically, the PCR-duplicated reads were marked, and base quality score recalibration was carried out during the processing of BAM files. We subjected the final BAM files obtained by merging reads from multiple lanes to variant calling. We detected germline and somatic mutations using HaplotypeCaller (v.4.1.2.0) and MuTect2 (v.4.1.2.0), respectively.

We considered mutations in the virus-transduced regions of both mice that were not detected in the untransduced regions of either mouse as having greater potential to be induced by genome editing. To detect germline mutations, we applied base quality score recalibration using single-nucleotide polymorphism and indel calls from v.3 of the Mouse Genome Project, which comprises genomic variants detected from 18 mouse strains⁵⁸. We estimated the frequencies of editing events at corresponding sites for each genomic DNA sample on the basis of the read counts of the modified and unmodified alleles stored in the VCF files. We used R programming (R studio; v.1.3.1056) to filter mutations that resided in the repetitive elements (UCSC repeatmasker mm10) and mutations that overlapped with the germline mutations. We annotated the presence of the genetic variants in the gene body from the Ensemble database obtained from the BioMart database (<http://m.ensembl.org/biomart>). We further designed somatic mutations that resided in exons and untranslated regions. We subsequently examined the expression levels of associated genes in brain cells by querying the cell-type-specific transcriptome dataset (Brain RNA-Seq)²⁵. We considered genes to be expressed in the brain if the number of fragments per kilobase of transcript per million mapped reads was greater than 1 in at least one brain cell type.

A β extraction, western blot analysis and ELISA. We sequentially extracted A β from the soluble and insoluble fractions of the dorsal hippocampi³⁵. We first homogenized frozen hippocampal tissues in tissue homogenization buffer (20 mM Tris-HCl (pH 7.4), 250 mM sucrose, 1 mM EDTA and 1 mM EGTA) with protease inhibitor cocktail (Sigma-Aldrich). We sequentially extracted soluble and insoluble A β by using diethylamine and formic acid, respectively. We analysed the levels of soluble and insoluble A β by western blot analysis. Moreover, we analysed soluble A β_{3-40} and A β_{3-42} using the V-PLEX A β Peptide Panel 1 (6E10) Kit (Meso Scale Discovery).

Immunohistochemistry. We anaesthetized the mice with pentobarbital and perfused them transcardially with Dulbecco's PBS (DPBS). We dissected the mouse brains, post-fixed them in 4% paraformaldehyde and sectioned them into 30 μ m sagittal brain slides using a free-floating vibratome (VT1000S, Leica) for immunohistochemistry. For 4G8 immunostaining, we performed antigen retrieval

with 70% formic acid. We then washed the brain sections three times with DPBS, blocked them with 2% goat serum and 0.3% Triton X-100 in DPBS⁵⁹ for 60 min at room temperature, and then incubated them with primary antibodies overnight at 4 °C.

We used the following primary antibodies: anti-HA tag antibody (1:50; 3724, Cell Signaling Technology); anti- $\text{A}\beta$, 17–24 antibody (1:1,000, clone 4G8, 800701, BioLegend); anti-Iba1 antibody (1:500, 019-19741, Wako); anti-GFAP antibody (1:5,000, 3670, Cell Signaling Technology); anti-PSD-95 antibody (1:500, ab2723, Abcam); anti-synaptophysin 1 antibody (1:500, 101011, Synaptic Systems); anti-LAMP-1 antibody (1:500, 1D4B, Developmental Studies Hybridoma Bank); and anti-NeuN antibody (1:100, MAB377, Millipore).

After we incubated the sections with primary antibodies, we washed them three times with DPBS and 0.3% Triton X-100 (DPBST). We then incubated the sections with secondary antibodies (anti-rabbit, anti-mouse or anti-rat Alexa Fluor 488, 546, 568 or 647; Thermo Fisher Scientific) in blocking buffer for 120 min at room temperature. After applying the corresponding secondary antibodies, we stained the brain sections with nuclear staining dye (4',6-diamidino-2-phenylindole (DAPI), 5 $\mu\text{g ml}^{-1}$) or SYTOX Green (1:30,000, S7020, Thermo Fisher Scientific) before mounting them onto slides.

For X34 amyloid-plaque staining, we incubated the brain sections in 1 μM X34 in X34 staining buffer (40% ethanol/60% DPBS mix; pH adjusted to 10) for 10 min at room temperature and then washed them three times with X34 staining buffer⁶⁰.

We performed imaging using a Leica DM6000 B compound microscope system and a Leica TCS SP8 confocal system.

Electrophysiology. We euthanized the mice, dissected their brains, and immediately transferred the brains to ice-cold oxygenated (95% O_2 /5% CO_2) artificial cerebrospinal fluid buffer. We subsequently prepared 300 μm brain slices by using a vibratome (HM650V; Thermo Fisher Scientific) and recovered them in artificial cerebrospinal fluid at 32 °C for at least 1 h. We recorded the CA1 fEPSPs using MED-P210A probes (Panasonic International) with a 100 μm interelectrode distance. After recording the baseline for 30 min, we induced LTP by 4 trains of theta-burst stimulation (10 brief bursts consisting of 4 pulses at 100 Hz)^{61,62}. We continued to record the fEPSPs for 60 min. Finally, we quantified the magnitude of LTP as the percentage change in the average slope of the fEPSP from 50–60 min after LTP induction.

Behavioural tests. For animal behavioural testing, we submitted the mice to the open-field test and Y-maze spontaneous alternation test, then let them rest for 2 months, and finally submitted them to the elevated plus maze test.

For the open-field test, we recorded the locomotor activity of the mice using a photobeam activity system and software (San Diego Instruments)⁶³. We placed each mouse in the centre of an open-top chamber (41 \times 41 \times 38 cm) and allowed the mouse to explore the chamber for 15 min each day for 3 consecutive days. The distance moved was recorded by the photobeams.

The spontaneous-alternation Y-maze test examines the spontaneous alternation performance of mice using a symmetrical Y-maze (30 cm long \times 20 cm high \times 8 cm wide)⁶³. Each mouse was habituated to the Y-maze environment 1 day before the test. On the test day, we placed each mouse into the centre of the Y-maze and allowed it to explore for 8 min. The sequence and total number of arms entered were recorded using EthoVision XT7 (Noldus). We calculated the percentage of alternation by dividing the number of consecutive entries into all 3 arms by the total number of arms entered minus 2. We did not count re-entry into the same arm for analysis.

Finally, the elevated plus maze test measures risk-taking behaviour using a plus-shaped maze elevated 60 cm above the floor. Four arms (30 cm long \times 5 cm wide), including two open arms and two closed arms with 15-cm-high walls, extend from the central platform. We placed each mouse on the central platform facing an open arm and allowed them to freely explore the maze for 5 min³⁹. The time the mice spent in each zone (closed arms, open arms or the central area) was recorded using EthoVision XT7 (Noldus).

Statistical analysis. All data are presented as mean \pm s.e.m., and n values indicate the number of individual experiments or mice. All statistical analyses were performed using GraphPad Prism (v6.01). The significance of differences was assessed by the paired or unpaired two-tailed Student's t -test and two-way repeated-measures analysis of variance (ANOVA) as indicated in the figure legends. We used the paired two-tailed t -test to analyse the intrahippocampal injections, because the comparison was between the uninjected and injected sides of the hippocampus within a single mouse. Two-way, repeated-measures ANOVA was performed to analyse habituation in the open-field test as a group comparison; the unpaired two-tailed t -test was performed in other instances. Intergroup differences were considered statistically significant at $*P < 0.05$, $**P < 0.01$ and $***P < 0.001$. No statistical methods were used to predetermine sample size. We randomly assigned the mice to different experimental groups. The investigators who performed the immunohistochemical, electrophysiological and behavioural tests were blinded to the genotypes of the mice and injection conditions. The quantification of immunohistochemical analysis was performed from 2–4 images of each brain section to eliminate any potential false-positive treatment effects.

Reporting Summary. Further information on research design is available in the Nature Research Reporting Summary linked to this article.

Data availability

The main data supporting the results in this study are available within the paper and its Supplementary Information. The raw data from whole-genome sequencing have been deposited in the NCBI Sequence Read Archive (SRA), with accession code PRJNA733582. The other raw and analysed datasets generated during the study are available for research purposes from the corresponding author on reasonable request, as they are too large to be publicly shared.

Received: 10 March 2020; Accepted: 8 June 2021;

References

- Cai, Y., An, S. S. & Kim, S. Mutations in presenilin 2 and its implications in Alzheimer's disease and other dementia-associated disorders. *Clin. Interv. Aging* **10**, 1163–1172 (2015).
- Campion, D. et al. Early-onset autosomal dominant Alzheimer disease: prevalence, genetic heterogeneity, and mutation spectrum. *Am. J. Hum. Genet.* **65**, 664–670 (1999).
- Cacace, R., Slegers, K. & Van Broeckhoven, C. Molecular genetics of early-onset Alzheimer's disease revisited. *Alzheimers Dement.* **12**, 733–748 (2016).
- Harper, P. S. The epidemiology of Huntington's disease. *Hum. Genet.* **89**, 365–376 (1992).
- Chio, A. et al. Global epidemiology of amyotrophic lateral sclerosis: a systematic review of the published literature. *Neuroepidemiology* **41**, 118–130 (2013).
- Selkoe, D. J. & Hardy, J. The amyloid hypothesis of Alzheimer's disease at 25 years. *EMBO Mol. Med.* **8**, 595–608 (2016).
- Ran, F. A. et al. Genome engineering using the CRISPR–Cas9 system. *Nat. Protoc.* **8**, 2281–2308 (2013).
- Serrano-Pozo, A., Frosch, M. P., Masliah, E. & Hyman, B. T. Neuropathological alterations in Alzheimer disease. *Cold Spring Harb. Perspect. Med.* **1**, a006189 (2011).
- Braak, H. & Braak, E. Frequency of stages of Alzheimer-related lesions in different age categories. *Neurobiol. Aging* **18**, 351–357 (1997).
- Ingusci, S., Verlengia, G., Soukupova, M., Zucchini, S. & Simonato, M. Gene therapy tools for brain diseases. *Front. Pharmacol.* **10**, 724 (2019).
- Chan, K. Y. et al. Engineered AAVs for efficient noninvasive gene delivery to the central and peripheral nervous systems. *Nat. Neurosci.* **20**, 1172–1179 (2017).
- Deverman, B. E. et al. Cre-dependent selection yields AAV variants for widespread gene transfer to the adult brain. *Nat. Biotechnol.* **34**, 204–209 (2016).
- Bedbrook, C. N., Deverman, B. E. & Gradinaru, V. Viral strategies for targeting the central and peripheral nervous systems. *Annu. Rev. Neurosci.* **41**, 323–348 (2018).
- Zeng, J. et al. TRIM9-mediated resolution of neuroinflammation confers neuroprotection upon ischemic stroke in mice. *Cell Rep.* **27**, 549–560.e6 (2019).
- Ortiz-Virumbrales, M. et al. CRISPR/Cas9-correctable mutation-related molecular and physiological phenotypes in iPSC-derived Alzheimer's PSEN2^{N141I} neurons. *Acta Neuropathol. Commun.* **5**, 77 (2017).
- Gyorgy, B. et al. CRISPR/Cas9 mediated disruption of the Swedish APP allele as a therapeutic approach for early-onset Alzheimer's disease. *Mol. Ther. Nucleic Acids* **11**, 429–440 (2018).
- Karczewski, K. J. et al. The mutational constraint spectrum quantified from variation in 141,456 humans. *Nature* **581**, 434–443 (2020).
- Wang, B. et al. γ -Secretase gene mutations in familial acne inversa. *Science* **330**, 1065 (2010).
- Mullan, M. et al. A pathogenic mutation for probable Alzheimer's disease in the APP gene at the N-terminus of β -amyloid. *Nat. Genet.* **1**, 345–347 (1992).
- Citron, M. et al. Excessive production of amyloid beta-protein by peripheral cells of symptomatic and presymptomatic patients carrying the Swedish familial Alzheimer disease mutation. *Proc. Natl Acad. Sci. USA* **91**, 11993–11997 (1994).
- Johnston, J. A. et al. Increased β -amyloid release and levels of amyloid precursor protein (APP) in fibroblast cell lines from family members with the Swedish Alzheimer's disease APP670/671 mutation. *FEBS Lett.* **354**, 274–278 (1994).
- Wiedenheft, B. et al. RNA-guided complex from a bacterial immune system enhances target recognition through seed sequence interactions. *Proc. Natl Acad. Sci. USA* **108**, 10092–10097 (2011).
- Gao, X. et al. Treatment of autosomal dominant hearing loss by in vivo delivery of genome editing agents. *Nature* **553**, 217–221 (2018).

24. Mashiko, D. et al. Generation of mutant mice by pronuclear injection of circular plasmid expressing Cas9 and single guided RNA. *Sci. Rep.* **3**, 3355 (2013).
25. Zhang, Y. et al. An RNA-sequencing transcriptome and splicing database of glia, neurons, and vascular cells of the cerebral cortex. *J. Neurosci.* **34**, 11929–11947 (2014).
26. Oakley, H. et al. Intraneuronal β -amyloid aggregates, neurodegeneration, and neuron loss in transgenic mice with five familial Alzheimer's disease mutations: potential factors in amyloid plaque formation. *J. Neurosci.* **26**, 10129–10140 (2006).
27. Kimura, R. & Ohno, M. Impairments in remote memory stabilization precede hippocampal synaptic and cognitive failures in 5XFAD Alzheimer mouse model. *Neurobiol. Dis.* **33**, 229–235 (2009).
28. Shao, C. Y., Mirra, S. S., Sait, H. B., Sacktor, T. C. & Sigurdsson, E. M. Postsynaptic degeneration as revealed by PSD-95 reduction occurs after advanced β and tau pathology in transgenic mouse models of Alzheimer's disease. *Acta Neuropathol.* **122**, 285–292 (2011).
29. Gowrishankar, S. et al. Massive accumulation of luminal protease-deficient axonal lysosomes at Alzheimer's disease amyloid plaques. *Proc. Natl Acad. Sci. USA* **112**, E3699–E3708 (2015).
30. Sharoar, M. G., Hu, X., Ma, X. M., Zhu, X. & Yan, R. Sequential formation of different layers of dystrophic neurites in Alzheimer's brains. *Mol. Psychiatry* **24**, 1369–1382 (2019).
31. Spires-Jones, T. L. & Hyman, B. T. The intersection of amyloid beta and tau at synapses in Alzheimer's disease. *Neuron* **82**, 756–771 (2014).
32. Woodhouse, A., West, A. K., Chuckowree, J. A., Vickers, J. C. & Dickson, T. C. Does β -amyloid plaque formation cause structural injury to neuronal processes? *Neurotox. Res.* **7**, 5–15 (2005).
33. Jankowsky, J. L. et al. Mutant presenilins specifically elevate the levels of the 42 residue β -amyloid peptide in vivo: evidence for augmentation of a 42-specific γ secretase. *Hum. Mol. Genet.* **13**, 159–170 (2004).
34. Garcia-Alloza, M. et al. Characterization of amyloid deposition in the APP^{Swe}/PS1^{ΔE9} mouse model of Alzheimer disease. *Neurobiol. Dis.* **24**, 516–524 (2006).
35. Fu, A. K. et al. IL-33 ameliorates Alzheimer's disease-like pathology and cognitive decline. *Proc. Natl Acad. Sci. USA* **113**, E2705–E2713 (2016).
36. Lalonde, R., Kim, H. D., Maxwell, J. A. & Fukuchi, K. Exploratory activity and spatial learning in 12-month-old APP^{695SWE}/co+PS1/ΔE9 mice with amyloid plaques. *Neurosci. Lett.* **390**, 87–92 (2005).
37. Choi, J. H. et al. Optimization of AAV expression cassettes to improve packaging capacity and transgene expression in neurons. *Mol. Brain* **7**, 17 (2014).
38. Patricio, M. I., Barnard, A. R., Orlans, H. O., McClements, M. E. & MacLaren, R. E. Inclusion of the woodchuck hepatitis virus posttranscriptional regulatory element enhances AAV2-driven transduction of mouse and human retina. *Mol. Ther. Nucleic Acids* **6**, 198–208 (2017).
39. Jawhar, S., Trawicka, A., Jenneckens, C., Bayer, T. A. & Wirths, O. Motor deficits, neuron loss, and reduced anxiety coinciding with axonal degeneration and intraneuronal A β aggregation in the 5XFAD mouse model of Alzheimer's disease. *Neurobiol. Aging* **33**, 196.e29–40 (2012).
40. Tible, M. et al. PKR knockout in the 5xFAD model of Alzheimer's disease reveals beneficial effects on spatial memory and brain lesions. *Aging Cell* **18**, e12887 (2019).
41. Ran, F. A. et al. In vivo genome editing using *Staphylococcus aureus* Cas9. *Nature* **520**, 186–191 (2015).
42. Cruts, M., Theuns, J. & Van Broeckhoven, C. Locus-specific mutation databases for neurodegenerative brain diseases. *Hum. Mutat.* **33**, 1340–1344 (2012).
43. Kleinstiver, B. P. et al. Broadening the targeting range of *Staphylococcus aureus* CRISPR–Cas9 by modifying PAM recognition. *Nat. Biotechnol.* **33**, 1293–1298 (2015).
44. Nagata, K. et al. Generation of *App* knock-in mice reveals deletion mutations protective against Alzheimer's disease-like pathology. *Nat. Commun.* **9**, 1800 (2018).
45. Park, H. et al. In vivo neuronal gene editing via CRISPR–Cas9 amphiphilic nanocomplexes alleviates deficits in mouse models of Alzheimer's disease. *Nat. Neurosci.* **22**, 524–528 (2019).
46. Filser, S. et al. Pharmacological inhibition of BACE1 impairs synaptic plasticity and cognitive functions. *Biol. Psychiatry* **77**, 729–739 (2015).
47. Ou-Yang, M.-H. et al. Axonal organization defects in the hippocampus of adult conditional BACE1 knockout mice. *Sci. Transl. Med.* **10**, ea05620 (2018).
48. Blume, T. et al. BACE1 inhibitor MK-8931 alters formation but not stability of dendritic spines. *Front. Aging Neurosci.* **10**, 229 (2018).
49. Ravindra Kumar, S. et al. Multiplexed Cre-dependent selection yields systemic AAVs for targeting distinct brain cell types. *Nat. Methods* **17**, 541–550 (2020).
50. Flytzanis, N. C. et al. Broad gene expression throughout the mouse and marmoset brain after intravenous delivery of engineered AAV capsids. Preprint at *bioRxiv* <https://doi.org/10.1101/2020.06.16.152975> (2020).
51. Bloch, D. B. et al. Sp110 localizes to the PML–Sp100 nuclear body and may function as a nuclear hormone receptor transcriptional coactivator. *Mol. Cell Biol.* **20**, 6138–6146 (2000).
52. Mo, W. & Zhang, J. T. Human ABCG2: structure, function, and its role in multidrug resistance. *Int. J. Biochem. Mol. Biol.* **3**, 1–27 (2012).
53. Liang, Z. et al. The pseudokinase CaMKv is required for the activity-dependent maintenance of dendritic spines. *Nat. Commun.* **7**, 13282 (2016).
54. Sun, J. et al. CRISPR/Cas9 editing of APP C-terminus attenuates β -cleavage and promotes α -cleavage. *Nat. Commun.* **10**, 53 (2019).
55. Hocquemiller, M., Giersch, L., Audrain, M., Parker, S. & Cartier, N. Adeno-associated virus-based gene therapy for CNS diseases. *Hum. Gene Ther.* **27**, 478–496 (2016).
56. Hudry, E. & Vandenberghe, L. H. Therapeutic AAV gene transfer to the nervous system: a clinical reality. *Neuron* **101**, 839–862 (2019).
57. Challis, R. C. et al. Systemic AAV vectors for widespread and targeted gene delivery in rodents. *Nat. Protoc.* **14**, 379–414 (2019).
58. Keane, T. M. et al. Mouse genomic variation and its effect on phenotypes and gene regulation. *Nature* **477**, 289–294 (2011).
59. Wojtowicz, J. M. & Kee, N. BrdU assay for neurogenesis in rodents. *Nat. Protoc.* **1**, 1399–1405 (2006).
60. Styren, S. D., Hamilton, R. L., Styren, G. C. & Klunk, W. E. X-34, a fluorescent derivative of Congo red: a novel histochemical stain for Alzheimer's disease pathology. *J. Histochem. Cytochem.* **48**, 1223–1232 (2000).
61. Seo, J. et al. Activity-dependent p25 generation regulates synaptic plasticity and A β -induced cognitive impairment. *Cell* **157**, 486–498 (2014).
62. Lee, K. et al. Replenishment of microRNA-188-5p restores the synaptic and cognitive deficits in 5XFAD mouse model of Alzheimer's disease. *Sci. Rep.* **6**, 34433 (2016).
63. Devi, L. & Ohno, M. Mitochondrial dysfunction and accumulation of the β -secretase-cleaved C-terminal fragment of APP in Alzheimer's disease transgenic mice. *Neurobiol. Dis.* **45**, 417–424 (2012).

Acknowledgements

We thank K. Liu, W.-Y. Fu, X. Wang, K.-W. Hung, C. Kwong, R. M. Delos Reyes, K. Cheung, N. Mullapudi, E. Tam, J. Zhang, H. Cao, S.-F. Li and P.-O. Chiu of the Hong Kong University of Science and Technology; and B. E. Deverman, K. Beadle and Y. Lei of California Institute of Technology for their excellent technical assistance. We are grateful to all members of the Ip laboratory for discussions. This study was supported in part by the National Key R&D Program of China (2018YFE0203600), the Guangdong Provincial Key S&T Program (2018B030336001), the Guangdong Provincial Fund for Basic and Applied Basic Research (2019B1515130004), the Hong Kong Research Grants Council Theme-based Research Scheme (T13-605/18-W), the Area of Excellence Scheme of the University Grants Committee (AoE/M-604/16), the Innovation and Technology Commission (ITCPD/17-9), the Lee Hysan Foundation (LHF17SC01), the Shenzhen Knowledge Innovation Program (JCYJ20180507183642005 and JCYJ20200109115631248), the Shenzhen–Hong Kong Institute of Brain Science–Shenzhen Fundamental Research Institutions (project number: 2019SHIBS0001), the HKUST-SIAT Joint Laboratory for Brain Science for technical platform support, and the Beckman Institute for CLARITY, Optogenetics and Vector Engineering Research for technology development and broad dissemination (clover.caltch.edu (V.G.) and the CZI Neurodegeneration Challenge Network (V.G.)).

Author contributions

Y.D., T.Y., A.K.Y.F. and N.Y.I. designed the research; Y.D., T.Y., Z.Q., A.M., X.Z., K.-C.L., Yuewen Chen and Yu Chen performed the research; Y.D., T.Y., A.K.Y.F. and N.Y.I. analysed the data; X.Z. performed bioinformatics analysis; V.G. and N.Y.I. contributed to the design and availability of reagents/analytical tools; and Y.D., T.Y., A.K.Y.F. and N.Y.I. wrote the paper with input from all authors.

Competing interests

The authors declare no competing interests.

Additional information

Supplementary information The online version contains supplementary material available at <https://doi.org/10.1038/s41551-021-00759-0>.

Correspondence and requests for materials should be addressed to N.Y.I.

Peer review information *Nature Biomedical Engineering* thanks Brandon Harvey, Brigitte van Zundert and the other, anonymous, reviewer(s) for their contribution to the peer review of this work. Peer reviewer reports are available.

Reprints and permissions information is available at www.nature.com/reprints.

Publisher's note Springer Nature remains neutral with regard to jurisdictional claims in published maps and institutional affiliations.

© The Author(s), under exclusive licence to Springer Nature Limited 2021

Reporting Summary

Nature Research wishes to improve the reproducibility of the work that we publish. This form provides structure for consistency and transparency in reporting. For further information on Nature Research policies, see [Authors & Referees](#) and the [Editorial Policy Checklist](#).

Statistics

For all statistical analyses, confirm that the following items are present in the figure legend, table legend, main text, or Methods section.

- | n/a | Confirmed |
|-------------------------------------|--|
| <input type="checkbox"/> | <input checked="" type="checkbox"/> The exact sample size (n) for each experimental group/condition, given as a discrete number and unit of measurement |
| <input type="checkbox"/> | <input checked="" type="checkbox"/> A statement on whether measurements were taken from distinct samples or whether the same sample was measured repeatedly |
| <input type="checkbox"/> | <input checked="" type="checkbox"/> The statistical test(s) used AND whether they are one- or two-sided
<i>Only common tests should be described solely by name; describe more complex techniques in the Methods section.</i> |
| <input checked="" type="checkbox"/> | <input type="checkbox"/> A description of all covariates tested |
| <input type="checkbox"/> | <input checked="" type="checkbox"/> A description of any assumptions or corrections, such as tests of normality and adjustment for multiple comparisons |
| <input type="checkbox"/> | <input checked="" type="checkbox"/> A full description of the statistical parameters including central tendency (e.g. means) or other basic estimates (e.g. regression coefficient) AND variation (e.g. standard deviation) or associated estimates of uncertainty (e.g. confidence intervals) |
| <input type="checkbox"/> | <input checked="" type="checkbox"/> For null hypothesis testing, the test statistic (e.g. F , t , r) with confidence intervals, effect sizes, degrees of freedom and P value noted
<i>Give P values as exact values whenever suitable.</i> |
| <input checked="" type="checkbox"/> | <input type="checkbox"/> For Bayesian analysis, information on the choice of priors and Markov chain Monte Carlo settings |
| <input checked="" type="checkbox"/> | <input type="checkbox"/> For hierarchical and complex designs, identification of the appropriate level for tests and full reporting of outcomes |
| <input checked="" type="checkbox"/> | <input type="checkbox"/> Estimates of effect sizes (e.g. Cohen's d , Pearson's r), indicating how they were calculated |

Our web collection on [statistics for biologists](#) contains articles on many of the points above.

Software and code

Policy information about [availability of computer code](#)

Data collection LAS X (Leica) was used for imaging; V-PLEX A β Peptide Panel 1 (6E10) Kit (Meso Scale Discovery) was used for ELISA; illumina HiSeq was used for deep sequencing; illumina NovaSeq was used for whole-genome sequencing.

Data analysis GraphPad Prism 6 was used for all statistical analysis and graphing; ImageJ (Version 1.51h) and MetaMorph Offline (Version 7.8.8.0), were used for image analysis; CRISPResso was used to analyze deep sequencing data; Trimmomatic (version 0.32), BWA mem (version 0.7.12-r1039), and Genome Analysis Toolkit (GATK) Best Practices (Version 4.1.2.0) were used to analyze whole-genome sequencing data.

For manuscripts utilizing custom algorithms or software that are central to the research but not yet described in published literature, software must be made available to editors/reviewers. We strongly encourage code deposition in a community repository (e.g. GitHub). See the Nature Research [guidelines for submitting code & software](#) for further information.

Data

Policy information about [availability of data](#)

All manuscripts must include a [data availability statement](#). This statement should provide the following information, where applicable:

- Accession codes, unique identifiers, or web links for publicly available datasets
- A list of figures that have associated raw data
- A description of any restrictions on data availability

The main data supporting the results in this study are available within the paper and its Supplementary Information. The raw data of whole-genome sequencing have been deposited in the NCBI Sequence Read Archive (SRA), with accession code PRJNA733582. The other raw and analyzed datasets generated during the study are available for research purposes from the corresponding authors on reasonable request as they are too large to be publicly shared.

Field-specific reporting

Please select the one below that is the best fit for your research. If you are not sure, read the appropriate sections before making your selection.

Life sciences Behavioural & social sciences Ecological, evolutionary & environmental sciences

For a reference copy of the document with all sections, see [nature.com/documents/nr-reporting-summary-flat.pdf](https://www.nature.com/documents/nr-reporting-summary-flat.pdf)

Life sciences study design

All studies must disclose on these points even when the disclosure is negative.

Sample size	No statistical methods were used to predetermine sample size. Sample sizes were determined on the basis of previous experimental experience and similar published studies.
Data exclusions	No data were excluded from the study.
Replication	Multiple mice were examined for each endpoint. All findings were reproduced in multiple mice with the same methodology.
Randomization	Transgenic mice were randomly selected for virus injection.
Blinding	The investigators were blinded to group allocation during data collection and analysis.

Reporting for specific materials, systems and methods

We require information from authors about some types of materials, experimental systems and methods used in many studies. Here, indicate whether each material, system or method listed is relevant to your study. If you are not sure if a list item applies to your research, read the appropriate section before selecting a response.

Materials & experimental systems

n/a	Involved in the study
<input type="checkbox"/>	<input checked="" type="checkbox"/> Antibodies
<input type="checkbox"/>	<input checked="" type="checkbox"/> Eukaryotic cell lines
<input checked="" type="checkbox"/>	<input type="checkbox"/> Palaeontology
<input type="checkbox"/>	<input checked="" type="checkbox"/> Animals and other organisms
<input checked="" type="checkbox"/>	<input type="checkbox"/> Human research participants
<input checked="" type="checkbox"/>	<input type="checkbox"/> Clinical data

Methods

n/a	Involved in the study
<input checked="" type="checkbox"/>	<input type="checkbox"/> ChIP-seq
<input checked="" type="checkbox"/>	<input type="checkbox"/> Flow cytometry
<input checked="" type="checkbox"/>	<input type="checkbox"/> MRI-based neuroimaging

Antibodies

Antibodies used	We used the following primary antibodies: anti-HA tag antibody (1:50; #3724,rabbit; #2367,mouse; Cell Signaling Technology); anti- β -amyloid, 17-24 antibody (1:1,000, clone 4G8, 800701, mouse, BioLegend); anti-Iba 1 antibody (1:500, 019-19741, rabbit, Wako); anti-GFAP antibody (1:5,000, #3670, mouse, Cell Signaling Technology); anti-PSD-95 antibody (1:500, ab2723, rabbit, Abcam); anti-synaptophysin 1 antibody (1:500, 101011, mouse, Synaptic Systems); anti-LAMP-1 antibody (1:500, 1D4B, rat, Developmental Studies Hybridoma Bank); and anti-NeuN antibody (1:100, MAB377, mouse, Millipore).
Validation	All antibodies were validated by the manufacturer or in relevant publications (Fu A., 2016, PNAS; FU A., 2014, PNAS; Tunc-Ozcan E., 2019, Nat Commu; Shikanai M., 2018 iScience; Andrejewski N., 1999, J Biol Chem).

Eukaryotic cell lines

Policy information about [cell lines](#)

Cell line source(s)	HEK293T cells from American Type Culture Collection (ATCC).
Authentication	None of the cell lines were authenticated.
Mycoplasma contamination	The HEK293T cells were tested, and confirmed to be negative.
Commonly misidentified lines (See ICLAC register)	No commonly misidentified cell lines were used.

Animals and other organisms

Policy information about [studies involving animals](#); [ARRIVE guidelines](#) recommended for reporting animal research

Laboratory animals

5XFAD transgenic mice, which harbour 5 familial AD mutations (APP K670N/M671L [Swedish], I716V [Florida], V717I [London], and PS1 M146L and L286V), and APP/PS1 transgenic mice, which harbour the APP K670N/M671L (Swedish) mutation and the PS1 exon-9 deletion, were obtained from the Jackson Laboratory (stock numbers: 008730 and 004462, respectively). For research, male transgenic mice and their wild-type littermates were used.

Wild animals

The study did not involve wild animals.

Field-collected samples

The study did not involve samples collected from the field.

Ethics oversight

The Animal Ethics Committee of the Hong Kong University of Science and Technology.

Note that full information on the approval of the study protocol must also be provided in the manuscript.